Power Generation on-board Aircraft using an Air-Powered Turbine Generator and Battery Interface System

Adél Coetzer
and Geoffrey Turner
Council for
Scientific and Industrial Research
PO Box 395, Pretoria, 0001
South Africa
Email: acoetzer@csir.co.za

Toit Mouton
Department of
Electrical and Electronic Engineering
Stellenbosch University
Private Bag X1, Matieland, 7602
Stellenbosch, South Africa
Email: dtmouton@sun.ac.za

Acknowledgments

The authors would like to thank the CSIR, in particular Adrian Adams, for allocating funding in support of the presented work.

Keywords

≪Hybrid power integration≫, ≪Adjustable speed generation system≫, ≪Converter control≫, ≪AC machine≫, ≪Generator excitation system≫, ≪Airplane≫, ≪Batteries≫.

Abstract

The design and implementation of a prototype hybrid power generation system, consisting of a ram air turbine (RAT) generator and an energy storage unit, is presented. The system is intended as a mechanism to supply additional or emergency power on-board an aircraft. Here we present the design, manufacture and testing of a synchronous rectifier required to interface an asynchronous generator to a dc bus. The dc bus connects to a battery of electrochemical cells through a bidirectional dc-dc converter. The dc-dc converter functions to regulate the dc bus voltage by utilising a double control loop strategy with an inner current control loop and outer voltage control loop. The power delivered to the dc bus from the generator is controlled as a function of the battery voltage, dc bus current and generator shaft speed. The control strategy used by the prototype circuit is presented in this paper along with simulation and experimental results.

Introduction

Additional power sources are required on-board modern aircraft, either to supply emergency power when the main power supply fails, or, in some instances, to provide continuous power to an additional electrical load. To this end, a ram air turbine (RAT) generator with an energy storage unit is presented. The RAT is driven by the airflow surrounding the sub-sonic aircraft and is the prime-mover of the generator shaft via a turbine wheel. The energy storage unit is typically employed to supply the peak (transient) power demanded by the load, while the turbine generator must deliver the combined average power demanded by the energy store and the electrical load [1].

A prototype circuit that demonstrates the flow of electrical power between an air-powered turbine generator, a battery of electrochemical cells, and an electrical load is presented. A three-phase squirrel-cage asynchronous induction machine is used as the generator. For laboratory testing the

generator was driven from an identical induction motor controlled by a commercial off-the-shelf variable-speed drive system, to simulate airflow through the turbine wheel (that would otherwise apply torque to the generator shaft). Series connected deep-cycle lead-acid batteries are used as the energy storage unit. The layout of the proposed circuit is shown in Fig. 1.

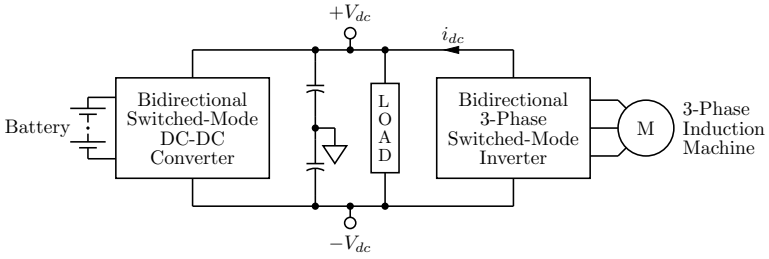

Fig. 1: Block diagram of battery and generator interface circuit.

The batteries are connected to a dc bus through a bidirectional switched-mode dc-dc converter and the induction machine interfaces with the dc bus through a bidirectional three-phase switched-mode dc-ac inverter. The interface is required to transfer up to 2 kW of electrical power between the induction generator and batteries. The load is connected between the positive and negative dc bus rails. The proposed nominal dc bus voltage is 350 V rail-to-rail.

The dc-dc converter is bidirectional to facilitate both the charging and discharging of the batteries, where the magnitude of the current to or from the batteries is regulated as a function of the dc bus voltage. The dc-ac inverter circuit functions as a synchronous rectifier to facilitate the flow of current from the induction generator to the dc bus whilst airborne. If the electrical load consumes more electrical power than the generator can deliver (at a given altitude and airspeed) then the batteries are observed to progressively discharge. This charge is replaced when the generator is able to supply power in excess of that demanded by the load, till such time as the batteries are fully charged.

Principal of Operation

The dc-dc converter topology is that of two bidirectional half-bridge circuits, one on top of the other, as shown in Fig. 2 with the midpoint grounded. Discrete MOSFETs are used as the switches for Q_1 through Q_4.

Twenty 12 V, 40 Ah rated deep-cycle lead-acid batteries are divided between the two half-bridge circuits, each using ten batteries indicated by V_{bat}. A positive inductor current i_L shown in Fig. 2 indicates that current is flowing from the dc bus into the batteries, thus charging the batteries. A negative inductor current indicates that current is flowing out of the batteries into the dc bus, typically into a load connected between the dc bus rails. During start-up a two-stage soft-start circuit limits the inrush current i_L from the batteries to the dc bus. The bidirectional dc-dc converter circuit regulates the dc bus voltage to 355 V rail-to-rail by sinking current to or sourcing current from the batteries.

The dc-ac inverter circuit connects to the regulated positive and negative dc bus rails at the output of the dc-dc converter. The dc-ac inverter circuit is based on the conventional three-phase half-bridge topology, as shown in Fig. 2. Provided the current i_{dc} is positive then the three-phase asynchronous machine operates as a generator. The generator is connected in a delta configuration as shown in Fig. 2.

The current i_{dc} supplied by the bidirectional inverter circuit to the dc bus is regulated as a function of the state of charge of the batteries, and is limited to a maximum mean value of 5.7 A by the inverter control circuit. This permits a power transfer of up to 2023 W from the generator to the nominal 355 V dc bus. The inverter control circuit reduces the generator

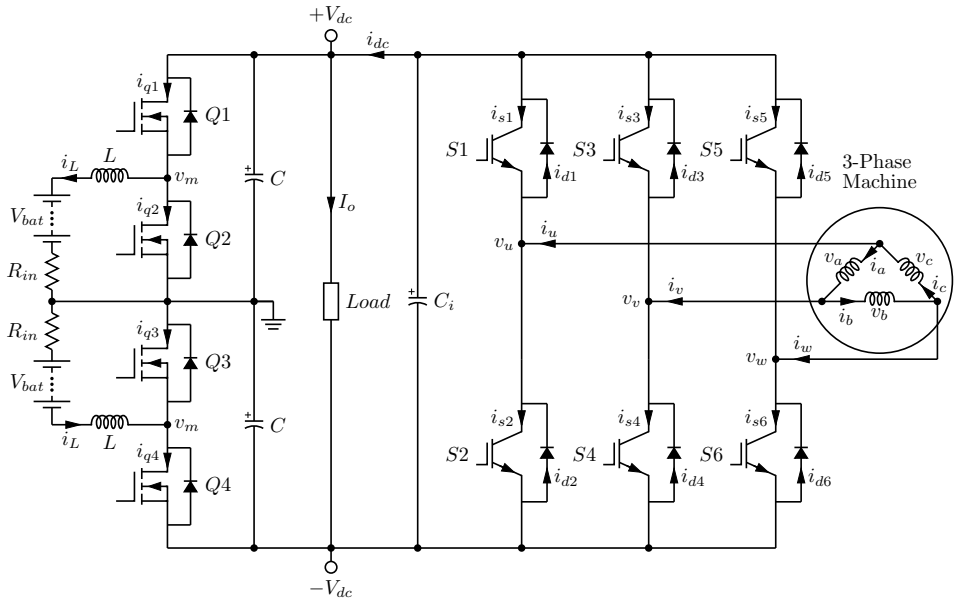

Fig. 2: Bidirectional dc-dc converter and dc-ac inverter interface circuit.

current (supplied to the dc bus) to zero once the batteries are charged to their optimal floating use voltage. The maximum electrical power that can be drawn from the generator is dictated by the mechanical power applied to the generator shaft, where the generator shaft speed varies as a function of the air mass-flow rate through the turbine (as a function of the aircraft speed and altitude) and the electrical load applied to the dc bus. The current in the generator windings is controlled such that it never exceeds the rated generator current, regardless of the generator shaft speed.

To control the frequency of the sinusoidal excitation applied to the three phases of the generator, the generator shaft speed ω_r is measured using a magnetic pick-up. The output signal from the magnetic pick-up is processed and input to a digital signal processor (DSP). The battery voltage is measured and, depending on the state-of-charge of the batteries, the current required to flow into the dc bus is determined and also input to the DSP. This value is subsequently scaled according to the measured frequency of the generator shaft to determine the magnitude of the sinusoidal modulator reference waveforms in accordance with the typical Volt/Hertz control method typically employed with variable speed asynchronous machines. The magnitude of the modulator reference waveforms output by the DSP are thus proportional to the magnitude of the fundamental component of the voltages applied to the generator stator terminals. Vector control is not required in this instance since the generator shaft speed does not change rapidly due to the large moment of inertia of the generator.

In order for the asynchronous machine to function as a generator it is required to operate at negative slip. In this instance the generator is specifically operated at a constant negative slip of -5.47 % and thus the frequencies of the three sinusoidal modulator reference voltages are approximately 5 % lower than the measured shaft speed. The modulator reference waveforms output by the DSP are subsequently compared to a triangular carrier wave to generate the required pulse-width modulation (PWM) signals for controlling the six IGBT switches employed in the inverter circuit.

Various safety features such as over-temperature, overvoltage and overcurrent protection are also included in the design of the dc-dc converter and dc-ac inverter control circuitry for the protection of the converters and generator.

Control System Design

The controllers for the dc-dc converter and dc-ac inverter function independently from each other. Both controllers assume an average model of the pulse-width modulator for s-domain frequency analysis.

DC-DC Converter Controller Design

Two control loops were implemented for the dc-dc converter circuit; an inner current control loop enclosed by an outer voltage control loop. The inner control loop regulates the mean converter inductor current I_L flowing to or from the batteries as a function of a set-point generated by the outer control loop. An active clamp circuit is used to limit the set-point in order to effectively limit the mean inductor current to ±10 A. The outer control loop regulates the dc bus voltage at the desired nominal voltage of 350 V by utilising the inner control loop to sink current from or source current to the dc bus. Both control loops use a pole-zero compensator. The closed-loop response of the inner current control loop is designed to be approximately 10 times faster than that of the outer voltage control loop to ensure stability.

In addition, a two-stage soft-start circuit (comprising pre- and post-charge mechanisms) [2] is used to increase the dc bus voltage gradually to the desired nominal rail-to-rail voltage to avoid excessive in-rush currents. The pre-charge circuit limits the peak battery in-rush current to 5 A by means of four parallel-connected 100 Ω resistors placed in series with each of the two battery banks. At such time as the bus capacitors C are charged to the equivalent battery potential (through the anti-parallel diodes of switch Q_1 and Q_4) the resistors are short-circuited by a relay to effectively remove the resistors from circuit. A resistor divider (connected across the dc bus), a reference voltage source and a comparator control the action of the relay.

The post-charge circuit is used to charge the dc bus from the equivalent battery potential to the respective +175 V and -175 V rails, and is designed to limit current spikes once the switches start switching. To achieve this the switch dead-time is progressively decreased from maximum (with all switches off) to some minimum value (where the minimum value was chosen to eliminate MOSFET shoot-through currents). In this way the on-times of the switches are gradually increased, progressively charging the dc bus while limiting the switch current.

DC-AC Inverter Controller Design

The dc-ac inverter control circuit modulates the voltages applied to the induction generator stator terminals and in return the generator supplies current to the dc bus through the dc-ac inverter circuit at a constant negative slip of -5.47 %. A block diagram of the proposed PWM control circuit is shown in Fig. 3.

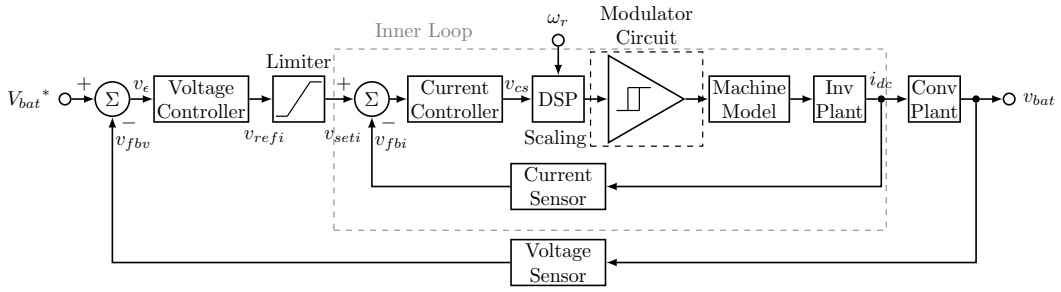

Fig. 3: Block diagram of the dc-ac inverter control circuit.

Once again, a double control loop approach is followed with an inner and outer control loop implemented. The inner loop controls the current supplied by the inverter to the dc bus as a function of a set-point v_{seti} generated by the outer control loop, where the outer control loop generates the set-point as a function of the state of charge of the batteries. The battery voltage

set-point $V_{bat}{}^{*}$ is a constant, corresponding to the recommended floating voltage of the twenty lead-acid batteries connected to the dc-dc converter circuit. As seen from Fig. 3, the current set-point v_{seti}, generated by the voltage control loop, is limited such that the average dc bus current (supplied by the inverter to the dc bs) is limited to a minimum of 0 A and a maximum of 5.7 A.

The control signal v_{cs} generated by the current control loop is input to an analogue-to-digital converter within the DSP, along with the generator shaft speed. The DSP generates the three sinusoidal modulator reference waveforms using a look-up table (LUT) approach similar to the approach followed in [3] and [4] where a part of the sinusoid is pre-computed and stored in the memory of the processor, thus forming a binary LUT. In Fig. 3 the PWM generation circuit is denoted as the modulator circuit which compares the modulator reference waveforms with a triangular carrier waveform.

The asynchronous machine was dynamically modelled using the well-known d-q transform where the three phase stator and rotor vector quantities were transformed into a synchronously rotating d-q reference frame [5],[6].

The plant portion of the dc-ac inverter circuit model is used to identify the relationship between the generator line voltages and the current flowing into the dc bus. Ignoring switching losses, it is reasonably assumed that the instantaneous power flowing into the dc bus equates to the instantaneous power flowing out of the generator. The dc bus current is thus calculated as a function of either the dc-ac inverter phase voltages and currents, or the generator line voltages and currents.

With reference to Fig. 2 the instantaneous power flowing into the dc bus is given by [7]

$$V_{dc(pp)} i_{dc} = v_a i_a + v_b i_b + v_c i_c, \tag{1}$$

where $V_{dc(pp)}$ is the regulated dc bus voltage of 355 V and i_{dc} is the time-varying dc bus current. The line currents are sinusoidal with a negligibly small ripple component, and can thus be viewed as pure sinusoids with only the fundamental components present.

The triangular carrier waveform's switching frequency is much higher than the fundamental frequency of the line voltages, resulting in a large frequency modulation ratio. Consequently, the amplitudes of the subharmonics are small and it may be reasonably assumed that only the fundamental frequency component of the line voltages will contribute towards the instantaneous power generated by the induction machine [7]. With the line voltages and currents approximated as fundamental line voltages and currents, (1) reduces to

$$\begin{aligned} i_{dc} &= \frac{2V_{s(rms)}I_{s(rms)}}{V_{dc(pp)}} [\cos(\omega_{s1}t)\cos(\omega_{s1}t+\phi) + \cos(\omega_{s1}t-120^\circ)\cos(\omega_{s1}t-120^\circ+\phi) \\ &\quad + \cos(\omega_{s1}t+120^\circ)\cos(\omega_{s1}t+120^\circ+\phi)] \\ &= \frac{3V_{s(rms)}I_{s(rms)}}{V_{dc(pp)}}\cos\phi, \end{aligned} \tag{2}$$

where $V_{s(rms)}$ and $I_{s(rms)}$ are the rms values of the fundamental line voltages and currents, respectively. The angle ϕ denotes the power factor angle. The rms values of the generator line voltages and currents are related by the equivalent generator impedance Z_{eq} such that

$$I_{s(rms)} = \frac{V_{s(rms)}}{|Z_{eq}|}, \tag{3}$$

where $|Z_{eq}|$ is the magnitude of the equivalent generator impedance. Recall that the amplitudes, and therefore also the rms values of the fundamental line voltages, are varied in proportion to the angular frequency of the fundamental waveforms (in accordance with typical Volt/Hertz control)

in order to maintain a constant rms flux within the ferromagnetic core of the asynchronous generator. The impedance Z_{eq} is also frequency dependant and thus, from (3), the rms value of the line currents will remain fairly constant, except at very low frequencies. With the rms line currents assumed constant, the dc bus current can thus be regulated as a function of the magnitude of the fundamental generator stator voltages.

A Hall-effect type current sensor is employed to provide the current feedback required by the inner control loop. The signal from the current sensor is processed and filtered using a low-pass filter to produce the feedback signal v_{fbi} shown in Fig. 3.

An integrator (which integrates the error between the measured and demanded dc bus current) is employed as the compensator for the current controller. This circuit is, however, prone to integral windup during transients, which can cause a large initial overshoot in the dc bus current, also leading to a slow settling time [8]. Since we require that the battery current is limited, in order to protect the batteries, a large dc bus current overshoot is undesirable, especially when accompanied by a prolonged settling time. To combat the integral windup, a tracking back anti-windup scheme [9] is employed.

The plant portion of the outer control loop, shown in Fig. 3, defines the relationship between the dc bus current and the battery voltage, as controlled by the dc-dc converter. The battery voltage is measured and scaled by a differential amplifier to provide the feedback voltage v_{fbv} shown in Fig. 3. A simple gain stage is used for the voltage controller shown in Fig. 3. Thus, as the battery voltage increases, the demanded dc bus current decreases. Some current, however small, will always be demanded by the controller in order to maintain the batteries at their floating potential.

The stability of the combined current and voltage control loops were examined in both the frequency and time domains. Time domain equations were derived, to which the Laplace transform was applied in order to derive the applicable frequency domain equations. A third order Padé approximation was included in the stability analysis of the current control loop to account for the time delay introduced by the DSP.

Simulation and Experimental Results

The dc-ac inverter and dc-dc converter circuits were manufactured and tested. The measured results were compared with the results of the simulated circuit.

Start-Up Response

The simulated dc-dc converter start-up response, showing both the instantaneous dc bus voltage and inductor current, are displayed in Fig. 4. This simulation includes the modelling of the two-stage soft-start circuit.

Fig. 4 indicates that the first stage of the soft-start circuit is predicted to be active for the first 350 ms after start-up, during which time the bus voltage rises from zero to the equivalent battery potential of 120 V per rail section. The in-rush current i_L charging the dc bus is seen to peak at 4.8 A.

At approximately 1.5 s the second stage of the soft-start circuit is activated, allowing the bus voltage to rise from 120 V to 175 V per rail section over the next 0.65 seconds. When the bus voltage reaches ±175 V there is a small voltage overshoot of 2 V per rail section, which is within the allowed dc bus operating range of 340 V to 360 V.

The large initial ripple voltage on the dc bus is caused by the post-charge circuit limiting the on-time of the switches. The ripple is predicted to decrease until it reaches a minimum peak-to-peak value of 27 mV once the soft-start circuit operation is terminated. The dc-dc converter's control circuitry then regulates the dc bus voltage to 350 V rail-to-rail continuously

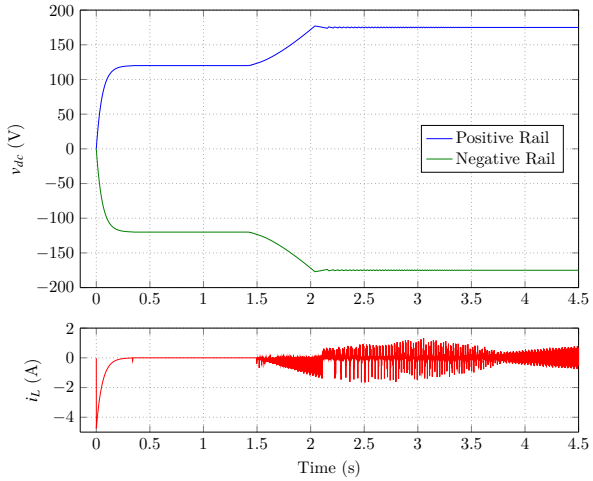

Fig. 4: Simulated dc bus voltage and inductor current during start-up.

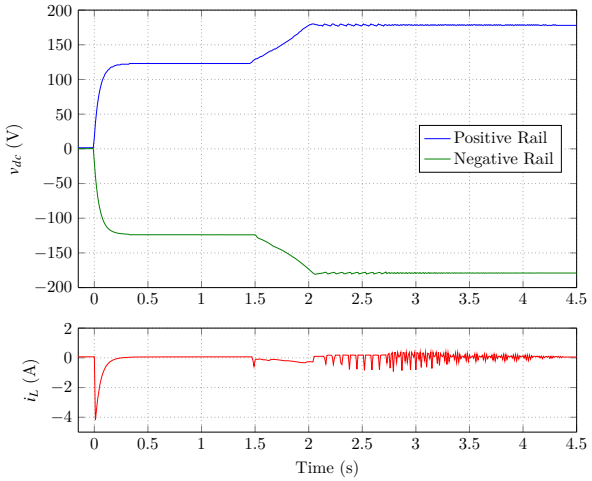

Fig. 5: Experimental result: Measured dc bus voltage and inductor current during start-up.

without any significant voltage ripple. As designed, the inductor current ripple is predicted to reach 2.25 A peak-to-peak.

Fig. 5 shows the measured dc bus voltage and inductor current during start-up. The magnitude and rate of change of the bus voltage is similar to the result of the time domain simulation shown in Fig. 4. Due to the sampling rate of the oscilloscope used to obtain the measurements (1000 samples over the chosen time period), the inductor current displayed in Fig. 5 is under sampled and thus aliasing occurs. Fig. 4 does however show a peak in-rush current of 4.6 A which closely matches the simulated current of 4.8 A.

The measured bus voltage is subsequently observed to rise to and regulate at 177.2 V and -177.8 V respectively, as shown in Fig. 5, over a period of approximately 0.6 s. The rail-to-rail nominal bus voltage is thus 355 V. The positive and negative dc bus voltages are observed to peak at 179 V and -180 V respectively. This corresponds to a voltage overshoot of approximately 2 V, as predicted by the time domain simulation. The positive and negative bus voltages are observed to regulate 2 to 3 V higher than the nominally required value of plus and minus 175 V due to a small inaccuracy in the set-point value of the dc bus.

System Operation Validation

Initially a 2 kW rated resistive load was connected between the 355 V regulated dc bus rails with zero torque applied to the generator shaft, leaving the dc-dc converter responsible for supporting the load. The dc-dc converter efficiency was determined by comparing the power delivered to the load to that drawn from the battery. The mean battery voltage was measured using a multimeter as 236.6 V and the average inductor current was measured with a LEM current probe as 9.592 A. An oscilloscope measurement of the instantaneous inductor current and ac coupled battery voltage showed that the current and voltage were in phase with each other. Simultaneously the regulated dc bus voltage was measured as 355 V rail-to-rail and the dc bus current flowing into the load as 6.01 A. The converter efficiency was calculated as

$$\eta = \frac{P_{out}}{P_{in}} = \frac{V_{dc} I_{dc}}{V_{bat} I_L} = 94.02\ \%. \tag{4}$$

To test the dc-ac inverter circuit, torque was applied to the generator shaft using an induction motor with variable speed drive unit. With the same load connected between the dc bus rails, the outer voltage control loop of the dc-ac inverter demands the maximum dc bus current to support the load. With the generator operated at negative slip the corresponding dc-ac inverter phase currents are shown in Fig. 6. The measured generator shaft frequency is, in this instance,

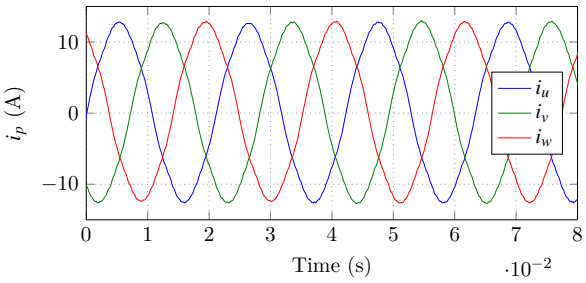

Fig. 6: Experimental result: Measured dc-ac inverter phase currents at a generator shaft frequency of 50 Hz.

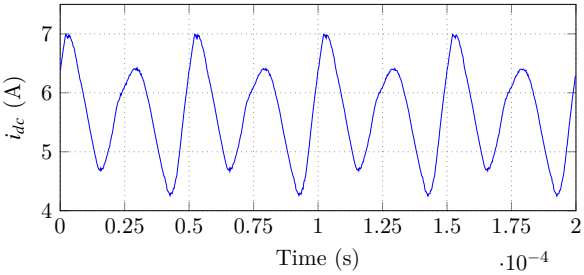

Fig. 7: Experimental result: Measured dc bus current with a 60 Ω load connected between the dc bus rails.

50 Hz, and the frequency of each of the dc-ac inverter phase currents is 47.4 Hz, indicating a slip of -5.47 %, as designed. The designed constant slip operation of the generator was further observed in the dc-ac inverter phase currents when tested at various shaft frequencies.

The corresponding measured dc bus current under steady-state conditions is shown in Fig. 7 at the maximum dc bus current set-point of 5.7 A. The mean value is measured as 5.66 A, which closely matches the desired value of 5.7 A. The error is due to a small inaccuracy in the current sensing circuit. The dc-ac inverter and generator circuit is thus able to supply 2 kW of electrical power to the dc bus.

The measured dc bus current is shown to have a fundamental frequency of 20 kHz with a 40 kHz component also present. The dc-ac inverter is switching at 20 kHz while the dc-dc converter is switching at 40 kHz accounting for the additional frequency component in Fig. 7.

Due to the difficulty in measuring the fundamental component of the inverter phase voltages and the absence of a power analyser from the laboratory, the dc-ac inverter efficiency was not determined.

When the load was removed from the dc bus, or the resistance of the load increased manually, current was observed to flow into the batteries and the battery voltage observed to begin to increase. Subsequently, less current is demanded by the voltage control loop and the battery voltage progressively settles. The batteries are further charged slowly and the mean dc bus current gradually decreases, under the control of the two control loops.

The implemented time domain simulation deals only with the electrical properties of the batteries, thus the batteries were modelled as a constant voltage source with an internal resistance. To provide a better approximation of the battery's response to the charging current, the battery voltage was approximated as a voltage source rising from 240 V (nominally 12 V per battery) to 265 V over a period of 3 s, after which the battery voltage was slowly increased to 272 V (floating use voltage of 13.6 V per battery) over the next 4 s. The result of this simulation is shown in Fig. 8.

Fig. 8 indicates that for the first 2.5 s of the simulation the current ramps up from zero in an effort to achieve the 5.7 A demanded by the set-point current. During this time the battery voltage is predicted to rise from 240 V to 260 V, after which the current set-point and predicted battery current converge, and are predicted to decrease in response to the increase in battery voltage. When the battery voltage reaches 265 V the batteries start charging at a lower rate. The current set-point is seen to also decline at this lower rate, with the dc bus current following its response. Once the battery voltage reaches the desired value of 272 V, the current set-point reaches zero, thus demanding zero current. The dc bus current is also seen to decrease to the desired value of 0 A. The time domain simulation predicts that both the voltage and current control loops of the dc-ac inverter are stable.

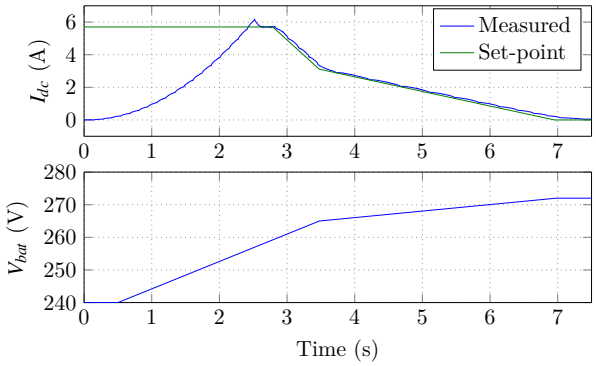

Fig. 8: Simulated dc bus current and battery voltage.

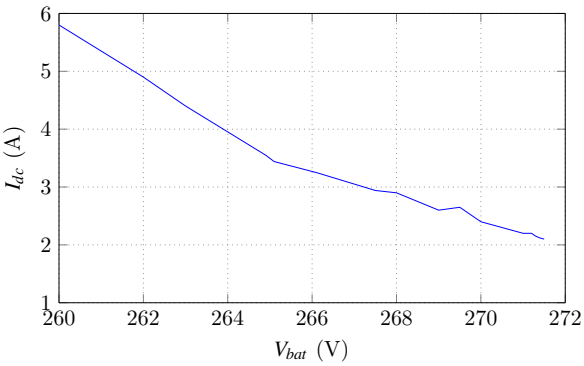

Fig. 9: Experimental result: Measured dc bus current vs battery voltage.

Due to the time duration required for the batteries to charge, the prototype circuit's measurement could not be obtained as a single measurement using an oscilloscope. The mean battery voltage and dc bus current were measured at regular intervals and the results are shown in Fig. 9. As soon as the generator started to deliver power to the dc bus (a load was not connected between the dc bus rails), the battery voltage was observed to increase rapidly to above 260 V. The results were taken from a battery voltage of 260 V as shown in Fig. 9. The measurements were taken with the batteries drained beforehand to their nominal value.

The results presented in Fig. 9 show the mean dc bus current does in fact decrease as the mean voltage of the batteries increases, as desired. Initially the dc bus current is seen to peak at 5.8 A while the dc bus voltage increases rapidly. The gain used in the voltage controller is sufficient to demand 5.7 A of current up to a measured battery voltage of 260 V. Thereafter the demanded current is observed to decreased, as shown in Fig. 9.

The current is observed to drop at approximately the designed rate until the battery voltage reaches 265 V. Thereafter the battery voltage progressively settles and requires more current than predicted to continue charging the batteries. From Fig. 9, the voltage is seen to never actually reach 272 V, remaining somewhere between 271 V and 272 V. Similarly the dc bus current is observed to reach a minimum value of approximately 2.1 A. The battery voltage and dc bus current thus reach equilibrium at these values. The equilibrium values were observed to be temperature dependent.

While the simulation predicted that the dc bus current would drop to zero at a battery voltage of 272 V, in practice, the battery voltage never actually reached 272 V, but does come close provided the necessary current is supplied to keep it there, thus trickle charging the batteries.

Conclusion

A circuit that demonstrates the interface between an asynchronous generator, a battery of electrochemical cells, and an electrical load was proposed for use on-board an aircraft. The successful design and implementation of a prototype circuit was presented. The measured start-up response of the dc-dc converter circuit was shown to compare well to the predicted start-up response. The converter also demonstrated a high efficiency and overall satisfactory performance.

The dc-ac inverter phase currents and dc bus current were presented in order to demonstrate the correct operation of the dc-ac inverter current control loop. Test results showing the relationship between the mean dc bus current and measured battery voltage were presented and the integration of the dc-dc converter and dc-ac inverter circuits were proven to be successful. The prototype circuit showed that the asynchronous generator can be controlled as a function of the dc-dc converter's battery voltage by making use of the presented dc-dc converter and

dc-ac inverter circuits. The system as a whole was shown to be stable with and without a load connected and provided the desired controller responses. In future work the generator will be driven by an air-powered turbine in preference to the induction motor with variable speed drive employed in the presented work.

References

[1] K. Rafal, B. Morin, X. Roboam, E. Bru, C. Turpin, and H. Piquet, "Hybridization of an aircraft emergency electrical network: Experimentation and benefits validation," in *2010 IEEE Vehicle Power and Propulsion Conference*, pp. 1–6, Sept 2010.

[2] W.-R. Liou, P.-H. Chen, and J.-C. Tzeng, "A synchronous boost regulator with pwm/pfm mode operation," in *ASIC, 2009. ASICON '09. IEEE 8th International Conference*, pp. 1066–1069, October 2009.

[3] K. K. Tan, H. X. Zhou, and T. H. Lee, "New interpolation method for quadrature encoder signals," *IEEE Transactions on Instrumentation and Measurement*, vol. 51, pp. 1073–1079, Oct 2002.

[4] H. V. Hoang and J. W. Jeon, "Signal compensation and extraction of high resolution position for sinusoidal magnetic encoders," in *Control, Automation and Systems, 2007. ICCAS '07. International Conference on*, pp. 1368–1373, Oct 2007.

[5] B. Bose, *Modern Power Electronics and AC Drives*, ch. 2 and 8, pp. 30–74, 334–413. Eastern Economy Edition, Prentice Hall PTR, 2002.

[6] B. Ozpineci and L. M. Tolbert, "Simulink implementation of induction machine model - a modular approach," in *Electric Machines and Drives Conference, 2003. IEMDC'03. IEEE International*, vol. 2, pp. 728–734, June 2003.

[7] N. Mohan, T. Undeland, and W. Robbins, *Power Electronics: Converters, Applications, and Design*. Power Electronics: Converters, Applications, and Design, John Wiley & Sons, third ed., 2003.

[8] G. Franklin, J. Powell, and A. Emami-Naeini, *Feedback control of dynamic systems*, pp. 633–636. International Edition, Pearson, sixth ed., 2010.

[9] X. Li, J. G. Park, and H. B. Shin, "Comparison and evaluation of anti-windup pi controllers," *Journal of Power Electronics*, vol. 11, no. 1, pp. 45–50, 2011.